RESEARCH PAPER

Surface Modification of Magnetic $MnFe_2O_4$@SiO_2 Core-shell Nanoparticles with Deposited Layer of 3-Aminopropyl Triethoxysilane

N. Akhlaghi, G. Najafpour-Darzi* and M. Mohammadi

* *najafpour@nit.ac.ir*

Received: June 2020 Revised: July 2020 Accepted: August 2020

* Biotechnology Research Laboratory, Faculty of Chemical Engineering, Babol Noshirvani University, Shariati Avenue, Babol, Iran

DOI: 10.22068/ijmse.17.4.77

Abstract: *Modification of $MnFe_2O_4$@SiO_2 core-shell nanoparticles with (3-aminopropyl) triethoxysilane (APTES) was investigated. The magnetite $MnFe_2O_4$ nanoparticles with an average size of ~30 nm were synthesized through a simple co-precipitation method followed by coating with silica shell using tetraethoxysilane (TEOS); that has resulted in a high density of hydroxyl groups loaded on nanoparticles. The prepared $MnFe_2O_4$@SiO_2 nanoparticles were further functionalized with APTES via a silanization reaction. For having suitable surface coverage of APTES, controlled hydrodynamic size of nanoparticles with a high density of amine groups on the outer surface, the APTES silanization reaction was investigated under different reaction temperatures and reaction times. Based on dynamic lightscattering (DLS) and zeta potential results, the best conditions for the formation of APTES-functionalized $MnFe_2O_4$@SiO_2 nanoparticles were defined at a reaction temperature of 70°C and the reaction time of 90 min. The effectiveness of our surface modification was established by X-ray photoelectron spectroscopy (XPS), transmission electron microscopy (TEM), Fourier transform infrared spectroscopy (FTIR), and vibrating sample magnetometer (VSM). The prepared magnetite nanostructure can be utilized as precursors to synthesize multilayered core-shell nanocomposite particles for numerous applications such as medical diagnostics, drug, and enzyme immobilization, as well as molecular and cell separation.*

Keywords: *APTES, Magnetite nanostructure, $MnFe_2O_4$ core-shell nanoparticles, Nanocomposite particles, Silanization, Silica shell.*

1. INTRODUCTION

The manganese ferrite ($MnFe_2O_4$) as a spinel ferrite material is among the most frequently utilized nanoparticles (NPs) in bio-related applications owing to its unique physicochemical properties including relative nontoxicity, biocompatibility, high saturation magnetization, and chemical stability [1, 2]. The applications of $MnFe_2O_4$ NPs in magnetic recording, medical diagnostics, magnetic hyperthermia, enzyme separation, and drug delivery, etc. have already been reported [3]. However, due to the high surface-to-volume ratio, the bare magnetite NPs possesses high surface free energies. For minimizing these energies, metal NPs tend to agglomerate in the physiological environment [4, 5]. Moreover, having high chemical reactivity leads to rapid and easy oxidation of magnetite NPs [4, 6, 7]. Effective surface functionalization of $MnFe_2O_4$ NPs with proper organic or inorganic materials can conquer these challenges and opens the possibility for further functionalization of NPs with desired bioactive molecules [6, 8].

3-aminopropyltriethoxysilane (APTES) as amino-organosilane exhibits bifunctional nature [9, 10] and has been widely used as a coupling agent for interaction with various molecules through amide binding. APTES surface-functionalized metal NPs possess extensive applications in various biological processes such as cell separation and diagnostic purposes like magnetic resonance imaging (MRI) [11]. Reddy et al. [12] used APTES for the functionalization of $MnFe_2O_4$@SiO_2 NPs with an amine group to be served as an adsorbent for separation of solids (Pt (IV)) from the aqueous phase. Shahrestani et al. [13] functionalized Fe_3O_4 NPs with APTES molecules for clarification of fruit juice *via* application of immobilized xylanase. Oliveira et al. [14] coated Ag@SiO_2 NPs with APTES for subsequent covalent interaction with the carboxylic group of ampicillin for combating bacterial antibiotic-resistant. The process of APTES silanization comprises two sequential steps: hydrolysis of the APTES ethoxy groups into hydroxyl groups and then, condensation of the hydroxyl groups with the hydroxyl presence on the surface of NPs. However, silanization

[DOI: 10.22068/ijmse.17.4.77]

reaction conditions strongly affect APTES structure and orientation [9]. Many reaction routes may participate in APTES conjugation resulted in either formation of a monolayer or complicated multilayer [10, 11]. Fig. 1 shows various possible interaction mechanisms of APTES molecules with the surface of silica-coated metal NPs, including horizontal polycondensation with hydroxyl groups from the surface of NPs (i), vertical polycondensation with neighboring silanes (ii), electrostatic attractions (iii), and hydrogen-bonding (iv) [10, 11].

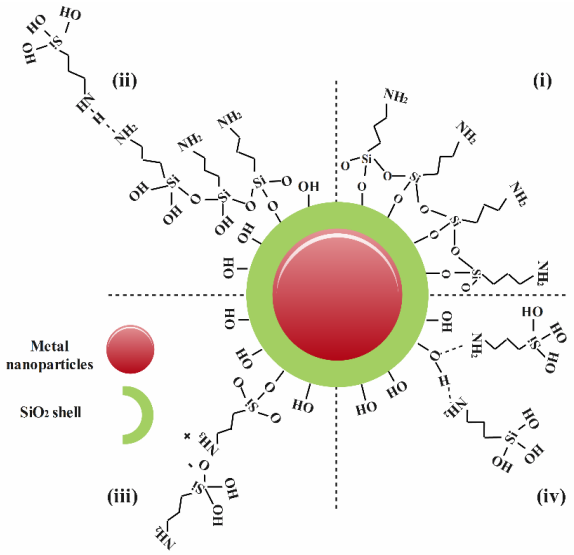

Fig. 1. Some typical bonding/interaction between APTES molecules and silica-coated metal NPs.

Despite the numerous literature conducted on optimization of reaction conditions for APTES functionalization onto silica surfaces [9, 10, 15], most of them are limited in scope, focused on modification of reaction conditions for APTES functionalization onto metal NPs. For improving the performance of amino silane functionalized-magnetite NPs, investigation on APTES silanization condition would assist to functionalize the surface of NPs by uniform deposition of APTES layer at the desired orientation.

The main objective of this work is to control the APTES layer quality on $MnFe_2O_4$-silica core-shell NPs under different reaction times and different reaction temperatures using a combination of dynamic light scattering (DLS) and zeta potential analyses. Zeta potential measurement was used to investigate the quality orientation of primary amino groups onto surfaces of nanoparticles. While the hydrolytic size of the APTES-functionalized NPs was controlled by DLS. Formation of $MnFe_2O_4$ nanocomposite particles with a large number of amine active sites provides great scope for the application of magnetite NPs for different purposes including enzyme immobilization and targeted drug delivery *via* covalent linkage.

2. MATERIALS AND METHODS

2.1. Materials

Ferric chloride hexahydrate ($FeCl_3.6H_2O$), magnesium chloride tetrahydrate ($MnCl_2.4H_2O$), hydrochloric acid (HCl), tetraethoxysilane (TEOS), 3-aminopropyltriethoxysilane (APTES), sodium hydroxide pellets (NaOH), and ammonium hydroxide, were purchased from Sigma-Aldrich. Ethanol (EtOH, 99.5%) was supplied by Scharlau. Milli-Q water was used throughout the experiment.

2.2. $MnFe_2O_4$ NPs Synthesis

$MnFe_2O_4$ NPs were prepared *via* co-precipitation method using Mn (II) and Fe (III) as precursors [7]. The reactants $FeCl_3.6H_2O$ and $MnCl_2.4H_2O$ were dissolved in Milli-Q water in a molar ratio of 2:1, respectively. Then, the solution of metal salts was added dropwise to an alkaline solution of 0.3 M NaOH at a temperature of 95 °C. After 2 h magnetic stirring, the prepared black solution was subjected to magnetic separation followed by three times washing with Milli-Q water and ethanol. Finally, the synthesized NPs were dried at 60 °C for 15 h.

2.3. $MnFe_2O_4$@SiO_2 NPs synthesis

The synthesis of $MnFe_2O_4$@SiO_2 core-shell NPs using TEOS was carried out in two steps. First, the prepared $MnFe_2O_4$ NPs (0.1 g) were acid-treated by dispersion of $MnFe_2O_4$ NPs in Milli-Q water (50 mL) and HCl (0.152 mL) for 10 min followed by washing three times with Milli-Q water. Second, the acid-treated $MnFe_2O_4$ NPs were dispersed in a mixture of ethanol (80 mL), Milli-Q water (20 mL), and aqueous ammonia solution (1 mL, 28 %) for 30 min [7]. Then, TEOS (0.3 mL) was dropwise added to the solution and the reaction was carried out for a duration of 6 h under agitation by a magnetic stirrer. Finally, the silica-coated $MnFe_2O_4$ NPs were washed three times with Milli-Q water and ethanol and then, dried at 60 °C for 15 h.

[DOI: 10.22068/ijmse.17.4.77]

2.4. APTES Silanization of $MnFe_2O_4$@SiO_2 NPs

For APTES silanization, the silica-coated $MnFe_2O_4$ NPs (0.1 g) were dispersed through sonication in a mixture of ethanol/water (20 mL, volume ratio of 1:1) for 30 min. Then, APTES at a fixed volume of 0.4 mL (2% v/v) was added to the solution of $MnFe_2O_4$@SiO_2 NPs [11]. For modification of APTES silanization, the solution of NPs was stirred under different reaction temperatures (20, 40, and 70 ˚C) at a fixed duration of 24 h. Then, the use of the defined temperature, the progress of silanization at a different reaction time of 90, 180, and 270 min was investigated. Finally, the $MnFe_2O_4$@SiO_2-NH_2 NPs were magnetically separated, washed three times with ethanol and then, dried at 60 ˚C for 15 h.

2.5. Characterization

X-ray photoelectron spectroscopy (XPS) was performed using Theta Probe Spectrometer (Thermo Fisher Scientific) using a monochromatic Al Kα excitation source (1486.6 eV). The morphology and size of the synthesized NPs were analyzed using a Transmission electron microscope (TEM, CM120 model, Philips Holland) with an accelerating voltage of 120 kV. X-ray diffraction (XRD) measurement was performed to identify the crystalline structures of $MnFe_2O_4$ NPs using CuKα radiation (X\'Pert Pro, Philips, Netherlands), between the 2θ range of 10˚ and 80˚. Dynamic light-scattering (DLS) and zeta potential of samples were measured in Milli-Q water (pH 7.0) using Zetasizer Nano-ZS (DLS, Malvern Instruments Inc. Worcestershire, UK). Infrared spectra (FTIR, Spectrum Two model, PerkinElmer) was recorded in the range of 650-4000 cm^{-1}. The analysis was performed with 5 mg of samples under nitrogen flow. The NPs were heated from room temperature to 980 ˚C, at a rate of 10 ˚C/ min. EDS Elemental analysis was performed using Energy dispersive spectroscopy (EDS, Sigma VP model, ZEISS, Germany). Vibrating Sample Magnetometer (VSM, Magnetic daghigh kavir, MDKB model, Iran) was used for the investigation of magnetic properties.

3. RESULTS AND DISCUSSION

The preparation process of $MnFe_2O_4$@SiO_2-NH_2 nanocomposite particles comprises of three steps (see Fig. 2). First, the $MnFe_2O_4$ NPs were synthesized through the co-precipitation method using $MnCl_2$ and $FeCl_3$ as precursors under alkaline conditions. Second, the prepared $MnFe_2O_4$ NPs were modified by the silica layer using hydrolysis of tetraethoxysilane (TEOS) molecules. The formation of TEOS layer provides advantages such as low NPs agglomeration, enhanced stability, improved hydrophilicity, and reduced toxicity which is the most critical aspect in the case of biomedical applications [16, 17]. Moreover, through this simple route, a core-shell nanostructure of $MnFe_2O_4$@SiO_2 with a high density of hydroxyl functional groups was formed which is desired for further interaction with APTES molecules. Finally, the binding modification of silane molecules (APTES) onto the surface of $MnFe_2O_4$@SiO_2 NPs was carried out under different reaction times and reaction temperatures to functionalized $MnFe_2O_4$@SiO_2 NPs with a high density of amine groups.

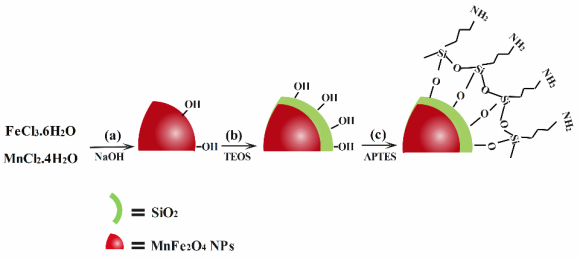

Fig. 2. Schematic illustration of $MnFe_2O_4$@SiO_2-NH_2 nanocomposite particles preparation: (a) synthesis of $MnFe_2O_4$ NPs, (b) formation of SiO_2 shell, and (c) synthesis of $MnFe_2O_4$@SiO_2-NH_2 NPs

3.1. Modification of APTES Silanization Reaction

The mechanism of APTES functionalization on $MnFe_2O_4$ NPs is based on two sequential reaction steps: in the first step, the ethoxy groups of APTES were hydrolyzed into hydroxyl groups. In the second step, the prepared hydroxyl groups interact with hydroxyl groups from the surface of NPs *via a* condensation process [11, 18]. The amount of APTES conjugated on NPs strongly affects the NPs' surface charge [19]. According to the zeta potential measurements, after modification of $MnFe_2O_4$@SiO_2 NPs with APTES, the mean zeta potential shift from negative to positive values due to the formation of primary amine functional groups on the surface of NPs.

[DOI: 10.22068/ijmse.17.4.77]

3.1.1. Effect of Temperature and Reaction Time on APTES Silanization

Temperature is a critical factor in the APTES silanization process [11]. As shown in Fig. 3a, at a fixed reaction time of 24 h, under silanization temperatures of 20, 40, and 70 ˚C, the surface charge of $MnFe_2O_4$@SiO_2 NPs changed from the initial value of -35 ± 2 mV to 11.2 ± 2, 18.9 ± 2, and 21.5 ± 2 mV, respectively. Based on obtained results, high temperature is in favor of the formation of amino-functionalized $MnFe_2O_4$@SiO_2 NPs. This is most probably due to an increase in APTES grafting density onto the surface of NPs at high temperature and consequently increase in the density of amine groups which is resulted in changes of zeta potential to a more positive value.

The higher silanization reaction temperature has also a positive effect on the hydrodynamic size of the amino-functionalized $MnFe_2O_4$@SiO_2 NPs. As shown in Fig. 3b, silanization at the reaction temperature of 20 ˚C caused an extensive increase in the particle size (1345 ± 2 nm) while the obtained results from zeta potential measurements confirmed low density of NH_2 groups functionalized onto the surface of $MnFe_2O_4$@SiO_2 NPs. This can be attributed to the fact that at the low reaction temperature, the mechanism of APTES conjugation on the surface of $MnFe_2O_4$@SiO_2 NPs changed; as a result, different reaction routes can be participating in APTES grafting. Therefore, instead of the formation of the MnFe-O-Si bond between the APTES molecule and metal NPs, APTES can be interacting with NPs through hydrogen bonding between the amino group of APTES and the hydroxyl functional groups on the surface of $MnFe_2O_4$@SiO_2 NPs [11] (see Fig. 1). Based on obtained results, the desired temperature of 70 ˚C was defined and the rest of the experiments were carried out at the designated temperature. Our results are consistent with data reported by Liu et al. [11] who demonstrated the temperature of 70 ˚C as the most suitable temperature for APTES silanization of iron NPs with the equilibrium grafting density of 301 mg/g.

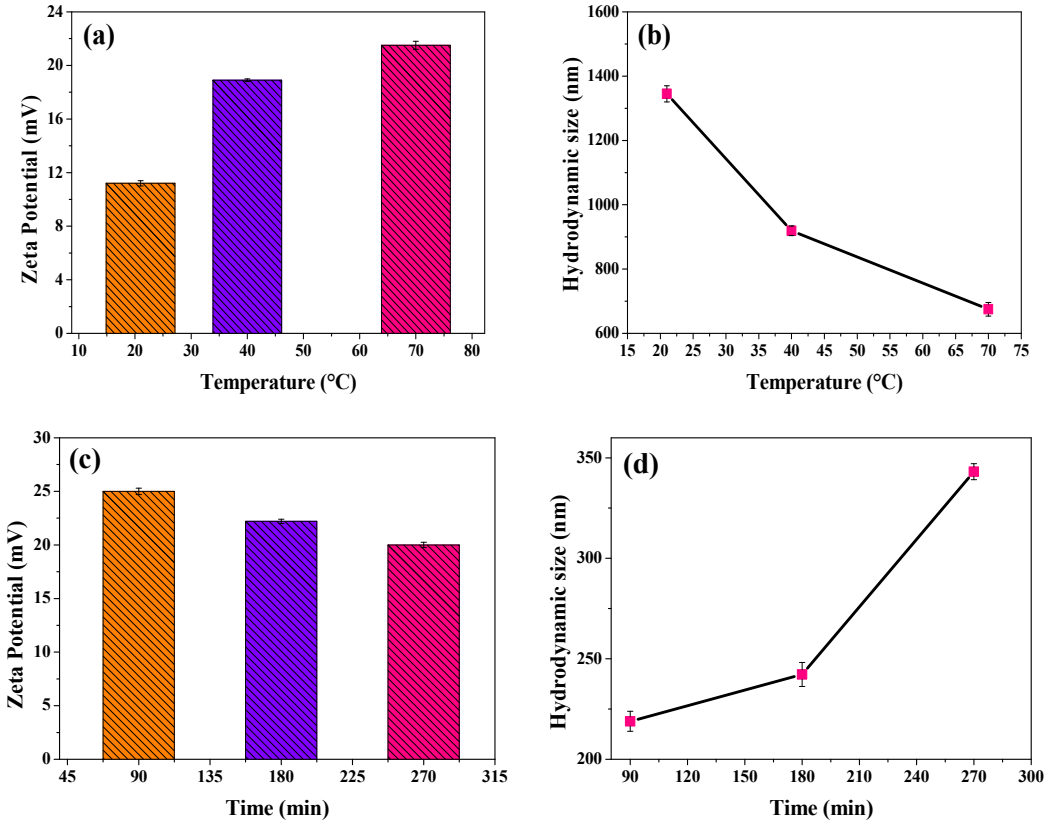

Fig. 3. Effect of APTES silanization temperature on the surface charge (a) and hydrodynamic size (b) of NPs; effect of APTES silanization time on the surface charge (c) and hydrodynamic size (d) of NPs, means ± SD (n=2)

[DOI: 10.22068/ijmse.17.4.77]

The effect of reaction time on APTES-functionalization of $MnFe_2O_4$@SiO_2 NPs was further investigated at the obtained temperature. Our results show that at low silanization reaction time, the zeta potential measurements displayed an increasing trend to a more positive value that indicates a certain increase of amino groups on the surface $MnFe_2O_4$@SiO_2 NPs (Fig. 3c). Also, reaction time has a significant influence on the final size of $MnFe_2O_4$@SiO_2-NH_2 NPs in the APTES silanization process. For the silanization reaction time of 90, 180, and 270 min, the hydrodynamic diameter of NPs by DLS analysis were 218.9 ± 3, 242.2 ± 3, and 343.1 ± 10 nm, respectively (see Fig. 3d). Based on these results, longer reaction time can result in the agglomeration of $MnFe_2O_4$@SiO_2 NPs and also the formation of a multilayer of APTES molecules with various orientations on the surface of NPs. The active surface area of NPs is reduced caused by high reaction time. APTES multilayer deposition happens on the agglomerated particles. Then, in the dispersion process, the size reduction may not occur in the functionalization process of NPs. So, APTES silanization at a reaction time of 90 min being preferred.

Overall, the surface charge of $MnFe_2O_4$ NPs changed from -29.9 ± 3 mV (Fig. 4a) to a more negative value of -35 ± 3 mV (data are not shown) after reaction with TEOS molecules which confirms the formation of more OH groups on the surface of NPs. APTES silanization of $MnFe_2O_4$@SiO_2 core-shell nanoparticles under the modified temperature of 70 ˚C and reaction time of 90 min led to changes in zeta potential to a positive value of 25 ± 3 mV (Fig. 4b).

Use of modified APTES silanization conditions, $MnFe_2O_4$@SiO_2-NH_2 NPs with uniform size distribution were obtained. As shown in Fig. 5, the average hydrodynamic size of $MnFe_2O_4$@SiO_2 NPs changed from 161.9 ± 0.5 nm (Fig. 5a) to 218.9 ± 3 nm (Fig. 5b) after conjugation of APTES molecules.

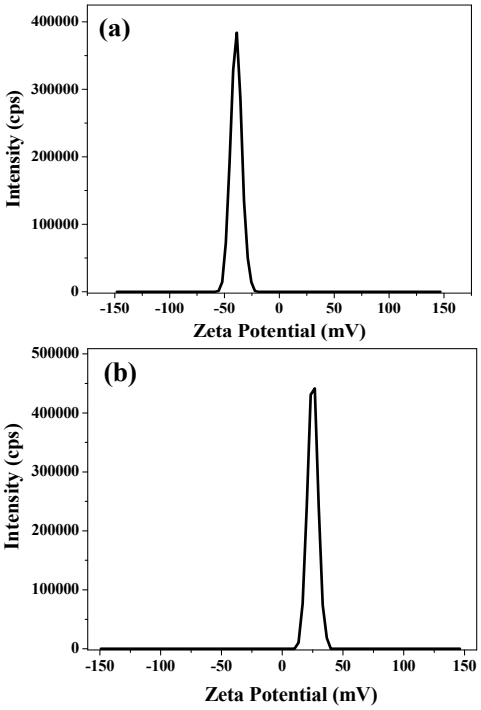

Fig. 4. zeta potential of (a) $MnFe_2O_4$ NPs and (b) $MnFe_2O_4$@SiO_2-NH_2 NPs

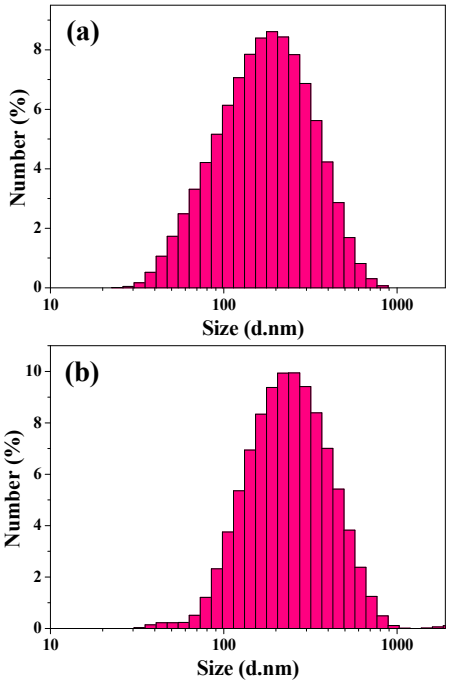

Fig. 5. hydrodynamic diameter of (a) $MnFe_2O_4$@SiO_2 NPs and (b) $MnFe_2O_4$@SiO_2-NH_2 NPs

[DOI: 10.22068/ijmse.17.4.77]

3.2. Characterization of the Prepared NPs

3.2.1. X-ray Photoelectron Spectroscopy (XPS) Analysis

XPS analysis was carried out to analyze the chemical composition of $MnFe_2O_4$ NPs and also validate the functionalization of $MnFe_2O_4$@SiO_2 NPs with APTES molecules. The XPS survey spectrum of the prepared $MnFe_2O_4$ NPs confirms the presence of Fe_{2p} (710 eV), Mn_{2sp} (640 eV), O_{1s} (529 eV), and C_{1s} (284 eV) (Fig. 6a). The atomic concentration of Fe_{2p}, Mn_{2p}, O_{1s}, and C_{1s} are 20.62 %, 3.31 %, 49.32 %, and 26.75 %, respectively. Fig. 6b shows the deconvoluted Fe_{2p} XPS spectrum, wherein the presence of two peaks with binding energy values of 711 eV and 725 eV referred to the $Fe_{2p3/2}$ and $Fe_{2p1/2}$ of Fe-O bonds, (typical for magnetite), respectively [20]. Moreover, satellite peaks at 717 eV and 731 eV ascribed to the Fe^{3+} oxidation state of iron species in $MnFe_2O_4$ NPs [21].

Mn_{2p} spectrum (Fig. 6c) has two characteristic peaks at 641 eV and 652.8 eV assigned to the $Mn_{2p\ 3/2}$ and $Mn_{2p\ 3/2}$ signals, respectively. One other additional peak at 644 eV was attributed to satellite peak [22]. The XPS survey spectrum of $MnFe_2O_4$@SiO_2-NH_2 NPs (Fig. 6d) confirms the presence of Si_{2p} (102 eV) assigned to APTES-modified Si and also silica shell formed on NPs using TEOS molecules, and N_{1s} (398 eV) corresponding to APTES nitrogen. The atomic concentrations of Si_{2p} and N_{1s} are 8.98 and 8.68 %, respectively. The deconvolution of the N_{1s} XPS spectrum (Fig. 6e) can be fitted with one broad peak at 398.7 eV, indicating the presence of the free NH_2 group of APTES on $MnFe_2O_4$@SiO_2 NPs [10]. In the Si_{2p} XPS spectrum (Fig. 6f), the peaks at 98.83 eV and 101.93 eV are attributed to bulk Si and SiO_2, respectively [9]. The results of XPS analyses confirm that the as-synthesized $MnFe_2O_4$ NPs were successfully functionalized with the APTES layer.

3.2.2. TEM and EDX Analyses

The structure, surface morphology, and size of the synthesized NPs were characterized by TEM analysis. Fig. 7a indicates the formation of the cubic shape of $MnFe_2O_4$ NPs. The average particle size of 30 nm was calculated by consideration of about 40 individual NPs of the TEM images. The histogram illustrating particles size distribution in the range of 10-60 nm (Fig. 7b, the size of the NPs was determined by measuring side lengths of NPs using Image J software). Fig. 7c depicts $MnFe_2O_4$@SiO_2-NH_2 NPs with high aggregation, because of the magnetic nature of manganese ferrite NPs. EDX analysis was further carried out to investigate the chemical composition of the synthesized $MnFe_2O_4$@SiO_2-NH_2 NPs. As shown in Fig. 7d,

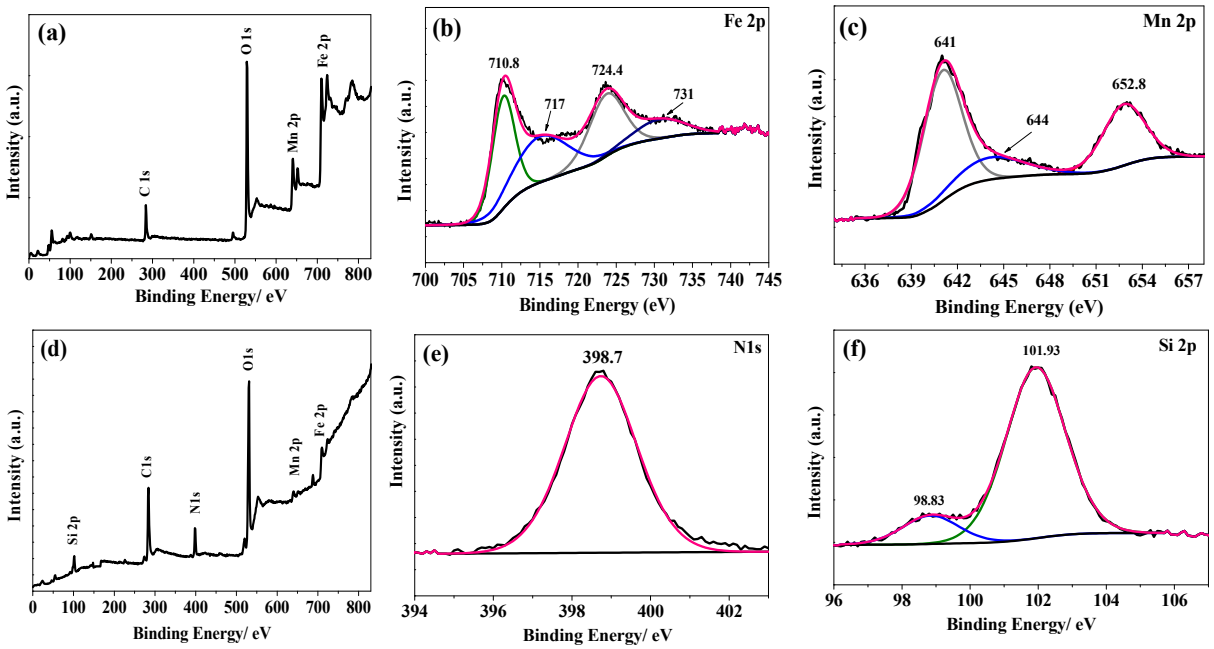

Fig. 6. XPS survey spectrum (a), high resolution of Fe_{2p} (b), and Mn_{2p} (c) spectra of $MnFe_2O_4$ NPs; XPS survey spectrum (d), high resolution of N_{1s} (e), and Si_{2p} (f) spectra of $MnFe_2O_4$@SiO_2-NH_2 NPs.

[DOI: 10.22068/ijmse.17.4.77]

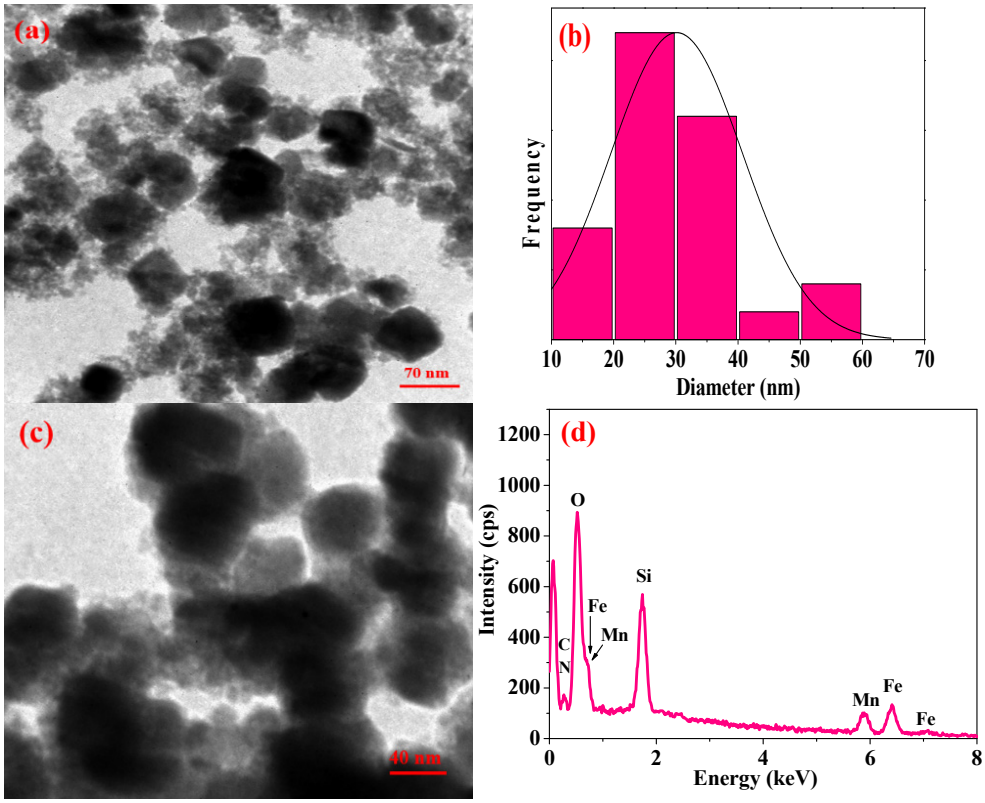

Fig. 7. TEM image (a) and size distribution of $MnFe_2O_4$ NPs (b), TEM image (c) and EDX spectrum (d) of $MnFe_2O_4$@SiO_2-NH_2 NPs.

the synthesized nanostructure is composed of Fe and Mn elements. The presence of the N signal is attributed to the amine group of APTES. Besides, the appearance of a strong peak at 1.74 keV validated the formation of silica shell on the $MnFe_2O_4$ NPs.

3.2.3. FTIR and VSM Analyses of the Samples

The chemical composition of $MnFe_2O_4$ NPs, $MnFe_2O_4$@SiO_2 NPs, and $MnFe_2O_4$@SiO_2-NH_2 NPs was further analyzed by FTIR. Fig. 8a (i) displays the FTIR spectrum of bare $MnFe_2O_4$ NPs, comprising vibration bands with peaks at 1630 and 3365 cm^{-1} attributed to OH groups [23]. The appearance of a sharp peak at 1067.5 cm^{-1} in the FTIR spectrum of $MnFe_2O_4$@SiO_2 NPs is attributed to the O-Si-O bending mode and Si-O-Si symmetric stretching mode of the coated silica shell (see Fig. 8a (ii)) [12].

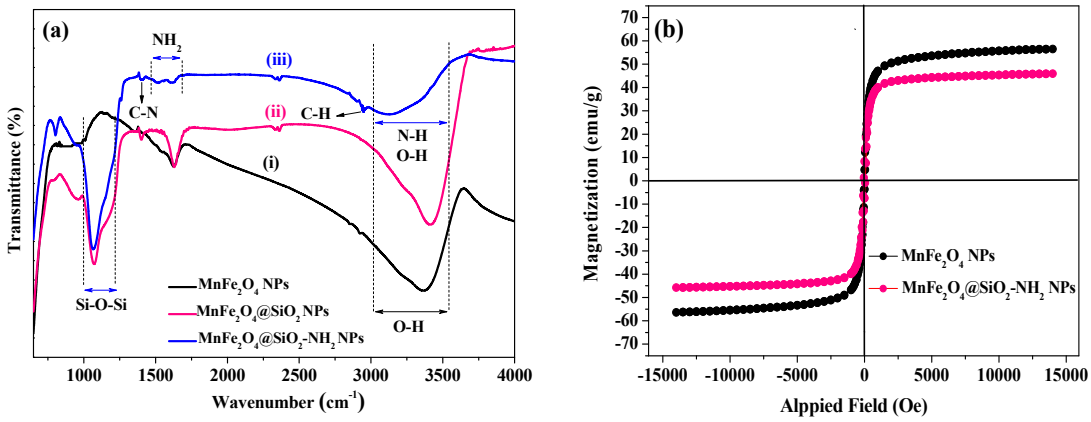

Fig. 8. (a) FTIR spectra of $MnFe_2O_4$ NPs (i), $MnFe_2O_4$@SiO_2 NPs (ii), and $MnFe_2O_4$@SiO_2-NH_2 NPs (iii); (b) hysteresis curves of $MnFe_2O_4$ NPs (black curve) and $MnFe_2O_4$@SiO_2-NH_2 NPs (pink curve).

[DOI: 10.22068/ijmse.17.4.77]

The FTIR spectrum of $MnFe_2O_4$@SiO_2-NH_2 NPs indicates the presence of Si-O stretching at 805.8 cm^{-1} (see Fig. 8a (iii)) [24]. The N-H stretching at 1518 cm^{-1} and the C-H asymmetric stretching at ~2940 cm^{-1} correspond to the aminopropyl from APTES [11, 12 and 23]. Moreover, the broadband at 3300 cm^{-1} corresponds to free amino groups (NH_2) of APTES on the surface of $MnFe_2O_4$@SiO_2 NPs which was overlain by hydroxyl groups [24]. The results of FTIR analyses confirm the formation of metal NPs with the NH_2 group terminal orientation.

The magnetization properties of $MnFe_2O_4$ NPs and $MnFe_2O_4$@SiO_2-NH_2 NPs were determined using VSM analysis at room temperature. Fig. 8b shows the hysteresis loop of samples, confirming the formation of metal NPs with the superparamagnetic property. According to obtained results, the bare $MnFe_2O_4$ NPs have saturation magnetization (Ms) of 56 emu/g. After modification of metal NPs with silica shell followed by APTES functionalization, Ms reduced to 46 emu/g which is principally attributed to the non-magnetic contribution of silica shell and APTES compounds on the surface of $MnFe_2O_4$ NPs.

3.3. X-Ray Diffraction (XRD) Measurement

The XRD pattern of $MnFe_2O_4$ NPs is displayed in Fig. 9. All observed characteristic diffraction peaks coincide with the standard database (JCPDS Card No. 01-073-1964), indicating cubic spinel phase magnetite [25]. Use of Scherrer's formula ($D= K \lambda /\beta \cos \theta$) the average crystalline size of $MnFe_2O_4$ NPs is about 19 ± 1 nm, based on the highest peak (311) positioned at 35.15°. As evidenced by XPS and XRD results, the synthesized $MnFe_2O_4$ NPs were pure with no additional bands of impurity.

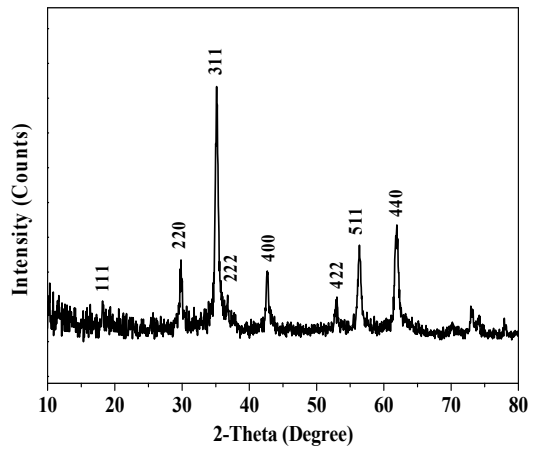

Fig. 9. X-ray diffraction pattern of $MnFe_2O_4$ NPs

4. CONCLUSION

The modification of $MnFe_2O_4$-silica core-shell NPs with amino silane was investigated to prepare magnetite NPs coated with a high density of primary amino groups and controlled hydrolytic size. APTES was used as amino silane agent and the process of silanization was carried out under different reaction temperatures and different reaction times. In summary, the surface charge of $MnFe_2O_4$@SiO_2 NPs was less sensitive to reaction time than the reaction temperature in the amino-functionalization process. The obtained results in this study demonstrated a positive effect of high temperature on the formation of amino silane layer on NPs with the desired orientation. In contrast, the efficiency of the silanization process was reduced at low reaction temperature due to the participation of different reaction routes in APTES conjugation. In addition, at high duration of APTES silanization reaction (higher than 90 min) not only the size of amino-functionalized $MnFe_2O_4$@SiO_2 NPs increased but also the density of amine groups on the surface of NPs decreased.

ACKNOWLEDGMENT

Authors gratefully acknowledge Babol Noshirvani University of Technology throughout the Ph.D. Research Grant No.: BNUT/ 945150001/98. This study is part of the Ph.D. thesis of Neda Akhlaghi, proposed and approved by the Faculty of Chemical Engineering, Noshirvani University of Technology, Babol, Iran.

REFERENCES

1. Pal, M., Rakshit, R. and Mandal, K., "Surface Modification of $MnFe_2O_4$ Nanoparticles to Impart Intrinsic Multiple Fluorescence and Novel Photocatalytic Properties". Appl. Mater. Interfaces, 2014, 6, 4903-4910.
2. Sen, S., Konar, S., Pathak, A., Dasgupta, S. and DasGupta, S., "Effect of Functionalized Magnetic $MnFe_2O_4$ Nanoparticles on Fibrillation of Human Serum Albumin". J. Phys. Chem. B., 2014, 118, 11667-11676.
3. Zhang, X.J., Wang, G.S., Cao, W.Q., Wei, Y.Z., Liang, J.F., Guo, L. and Cao, M.S.,

[DOI: 10.22068/ijmse.17.4.77]

"Enhanced Microwave Absorption Property of Reduced Graphene Oxide (RGO)-$MnFe_2O_4$ Nanocomposites and Polyvinylidene Fluoride". Appl. Mater. Interfaces, 2014, 6, 7471-7478.
4. Wei, W., He, Q. and Jiang, C., "Magnetic Iron Oxide Nanoparticles: Synthesis and Surface Functionalization Strategies". Nanoscale. Res. Lett., 2008, 3, 397-415.
5. Esmaeilia, A. and Ghobadianpour, S., "Vancomycin loaded superparamagnetic $MnFe_2O_4$ nanoparticles coated with PEGylated chitosan to enhance antibacterial activity". Int. J. Pharm., 2016, 501, 326-330.
6. Zhu, N., Ji, H., Yu, P., Niu, J., Farooq, M.U., Akram, M.W., Udego, I.O., Li, H. and Niu, X., "Surface Modification of Magnetic Iron Oxide Nanoparticles". Nanomaterials, 2018, 8, 810.
7. Rashid, Z., Soleimani, M., Ghahremanzadeh, R., Vossoughi, M. and Esmaeili, E., "Effective surface modification of $MnFe_2O_4$@SiO_2@PMIDA magnetic nanoparticles for rapid and high-density antibody immobilization". Appl. Surf. Sci., 2017, 426, 1023-1029.
8. Demin, A.M., Pershina, A.G., Minin, A. S., Mekhaev, A.V., Ivanov, V.V., Lezhava, S.P., Zakharova, A.A., Byzov, I.V., Uimin, M.A., Krasnov, V.P. and Ogorodova, L.M., "PMIDA- Modified Fe_3O_4 Magnetic Nanoparticles: Synthesis and Application for Liver MRI". Langmuir, 2018, 34, 3449-3458.
9. Acres, R.G., Ellis, A.V., Alvino, J., Lenahan, C.E., Khodakov, D.A., Metha, G.F. and Andersson, G.G., "Molecular Structure of 3-Aminopropyltriethoxysilane Layers Formed on Silanol-Terminated Silicon Surfaces". J. Phys. Chem. C., 2012, 116, 6289-6297.
10. Zhu, M., Lerum, M.Z. and Chen, W., "How To Prepare Reproducible, Homogeneous, and Hydrolytically Stable Aminosilane-Derived Layers on Silica". Langmuir, 2012, 28, 416-423.
11. Liu, Y., Li, Y., Li, X.M. and He, T., "Kinetics of (3-Aminopropyl) triethoxylsilane (APTES) Silanization of Superparamagnetic Iron Oxide Nanoparticles". Langmuir, 2013, 29, 15275-15282.
12. Reddy, D.H.K., Wei, W., Shuo, L., Song, M.H. and Yun, Y.S., "Fabrication of stable and regenerable amine functionalized magnetic nanoparticles ($MnFe_2O_4$@SiO_2-NH_2) as a potential material for Pt(IV) recovery from acidic solutions". ACS. Appl. Mater. Interfaces, 2017, 9, 18650-18659.
13. Shahrestani, H., Taheri-Kafrani, A., Soozanipour, A. and Tavakoli, O., "Enzymatic clarification of fruit juices using xylanase immobilized on 1, 3, 5-triazine-functionalized silica-encapsulated magneticnanoparticles". Biochem. Eng. J., 2016, 109, 51-58.
14. Oliveira, J.F.A., Saito, A., Bido, A.T., Kobarg, J., Stassen, H.K. and Cardoso. M. Borba., "Defeating Bacterial Resistance and Preventing Mammalian Cells Toxicity through Rational Design of Antibiotic-Functionalized Nanoparticles". Sci. Rep., 2017, 7, 1326.
15. Smith, E.A. and Chen, W., "How to Prevent the Loss of Surface Functionality Derived from Aminosilanes". Langmuir, 2008, 24, 12405-12409.
16. Ansari, S.A.M.K., Ficiara, E., Ruffinatti, F.A., Stura, I., Argenziano, M., Abollino, O., Cavalli, R., Guiot, C. and Agata, F.D., "Magnetic Iron Oxide Nanoparticles: Synthesis, Characterization and Functionalization for Biomedical Applications in the Central Nervous System". Materials, 2019, 12, 465.
17. Zhao, J.F., Wang, T., Lin, J.P., Yang, L.R. and Wu, M.B.P., "Preparation of High-purity 1, 3-Diacylglycerol Using Performance-enhanced Lipase Immobilized on Nanosized Magnetite Particles". Biotechnol. Bioproc. E., 2019, 24, 326-336.
18. Qiao, B., Wang, T.J., Gao, H. and Jin, Y., "High density silanization of nano-silica particles using-aminopropyltriethoxysilane (APTES)". Appl. Surf. Sci., 2015, 351, 646-654.
19. Cabanas, M.V., Lozano, D., Torres-Pardo, A., Sobrino, C., González-Calbet, J., Arcos, D. and Vallet-Regi, M., "Features of aminopropyl modified mesoporous silica nanoparticles.on the active targeting capability". Mater. Chem. Phys., 2018, 220, 260-269.
20. Demin, A.M., Mekhaev, A.V., Esin, A.A., Kuznetsov, D.K., Zelenovskiy, P.S., Shur, V.Y. and Krasnov, V.P., "Immobilization of PMIDA on Fe_3O_4 magnetic nanoparticles surface: mechanism of bonding". Appl. Surf. Sci., 2018, 440, 1196-1203.

[DOI: 10.22068/ijmse.17.4.77]

21. Yadav, R.S., Kuritka, I., Vilcakova, J., Jamatia, T., Machovsky, M., Skoda, D., Urbánek, P., Masař, M., Urbánek, M., Kalina, L. and Havlica, J., "Impact of Sonochemical Synthesis Condition on the Structural and Physical Properties of $MnFe_2O_4$ Spinel Ferrite Nanoparticles". Ultrason. Sonochem, 2019, 61, 104839.
22. Bongu, C.S., Ragupathi, J. and Nallathamby, K., "Exploration of MnFeO3/Multiwalled Carbon Nanotubes Composite as Potential Anode for Lithium Ion Batteries". Inorg. Chem., 2016, 55, 11644-11651.
23. Wang, H.Q., Yao, Z., Sun, Y., Zhou, Z., Xiong, Q. and Zhong, Z.X., "Immobilization of γ-glutamyltranspeptidase on Silylated Mesoporous TiO2 Whiskers". Biotechnol. Bioproc. E., 2014, 19, 304-310.
24. Hu, B., Pan, J., Yu, H.L., Liu, J.W. and Xu, J.H., "Immobilization of Serratia marcescens lipase onto amino-functionalized magnetic nanoparticles for repeated use in enzymatic synthesis of Diltiazem intermediate". Process. Biochem., 2009, 44, 1019-1024.
25. Khaleghi, M., Moradmard, H. and Shayesteh, S.F., "Cation Distributions and Magnetic Properties of Cu-Doped Nanosized $MnFe_2O_4$ Synthesized by the Coprecipitation Method". IEEE. Trans. Magn., 2018, 54, 1-5.

[DOI: 10.22068/ijmse.17.4.77]